Biomed Microdevices (2009) 11:915–924
DOI 10.1007/s10544-009-9308-6

Flexible microfluidic devices supported by biodegradable insertion scaffolds for convection-enhanced neural drug delivery

Conor P. Foley · Nozomi Nishimura · Keith B. Neeves · Chris B. Schaffer · William L. Olbricht

Published online: 8 April 2009

Abstract Convection enhanced delivery (CED) can improve the spatial distribution of drugs delivered directly to the brain. In CED, drugs are infused locally into tissue through a needle or catheter inserted into brain parenchyma. Transport of the infused material is dominated by convection, which enhances drug penetration into tissue compared with diffusion mediated delivery. We have fabricated and characterized an implantable microfluidic device for chronic convection enhanced delivery protocols. The device consists of a flexible parylene-C microfluidic channel that is supported during its insertion into tissue by a biodegradable poly(DL-lactide-*co*-glycolide) scaffold. The scaffold is designed to enable tissue penetration and then erode over time, leaving only the flexible channel implanted in the tissue. The device was able to reproducibly inject fluid into neural tissue in acute experiments with final infusate distributions that closely approximate delivery from an ideal point source. This system shows promise as a tool for chronic CED protocols.

Keywords Convection-enhanced delivery · Flexible neural implant · Microfluidics · Drug delivery

C. P. Foley · W. L. Olbricht (✉)
School of Chemical and Biomolecular Engineering,
Cornell University,
Ithaca, NY 14853, USA
e-mail: wlo1@cornell.edu

N. Nishimura · C. B. Schaffer · W. L. Olbricht
Department of Biomedical Engineering, Cornell University,
Ithaca, NY 14853, USA

K. B. Neeves
Chemical Engineering Department, Colorado School of Mines,
Golden, CO 80401, USA

1 Introduction

Convection enhanced delivery (CED) is a promising new technique for treating neurological disorders. In CED drugs are infused directly into tissue through a needle or catheter (Bobo et al. 1994). This technique circumvents the blood brain barrier and can achieve high local concentrations of drug with fewer side effects than with systemic delivery. Because many agents delivered directly to the brain are subject to rapid elimination from the interstitial space via permeation through the capillaries or metabolism within brain tissue (Haller and Saltzman 1998), drugs delivered by diffusion from polymer implants or bolus injections are often only able to penetrate a small distance, typically 1–3 mm from the implant (Walter et al. 1994; Krewson and Saltzman 1996). Since drug transport in CED is driven by an imposed pressure gradient rather than by diffusion along a concentration gradient, drugs can penetrate farther into tissue from the delivery site. Many compounds have been delivered in both animal and human experiments using CED. For example, infusions of small molecules (Bobo et al. 1994; Lonser et al. 1999; Groothuis et al. 1999), proteins (Laske et al. 1997; Lieberman et al. 1995, Lonser et al. 2002), growth factors (Hamilton et al. 2001; Yang et al. 2002), and nucleotides (Groothuis et al. 2000) have been examined in animals, and chemotherapy drugs (Mardor et al. 2001; Lidar et al. 2004), proteins (Kunwar et al. 2007; Sampson et al. 2003; Weber et al. 2003), and viral vectors (Worgall et al. 2008; Ren et al. 2003) have been administered in humans.

However, current CED protocols that use standard needles and catheters are not suitable for chronic applications for several reasons, including complications associated with tissue damage upon insertion, backflow of infusate along the needle path, occlusion of the needle tip by tissue,

and the tissue's foreign body response to the needle. Microfabricated devices offer many potential advantages over standard needles. Primarily, their small size reduces tissue damage upon insertion (Szarowski et al. 2003) and inhibits backflow (Morrison et al. 1999). Also, it is possible to locate the fluidic outlet away from the leading edge of the device to reduce occlusion of the fluidic channel. Furthermore, with current microfabrication technology it is possible to create devices with features that are not available in standard needles, e.g. recording and stimulating electrodes, chemical and mechanical sensors that could allow the device to respond to changes in the tissue environment, and multi-channel fluidics for delivering different compounds in a controlled regimen (Neeves et al. 2007).

Several researchers have created microfluidic silicon probes for use in the brain. Although these devices moderate backflow and reduce the initial tissue damage due to insertion (Chen et al. 1997; Rathnasingham et al. 2004; Neeves et al. 2006), they may not be particularly well suited for chronic implantation as the brittle nature of silicon increases the risk of a probe breaking inside the tissue. In addition, silicon probes have been found to cause a significant foreign body response (Szarowski et al. 2003; Turner et al. 1999). Studies have suggested that a flexible implant may elicit a reduced foreign body response compared to a rigid device by reducing the mechanical mismatch between the implant and the tissue (Rousche et al. 2001; Subbaroyan et al. 2005; Kim et al. 2004).

Researchers have shown that flexible catheters perform better than rigid catheters in chronic infusion studies in rats. Guarnieri et al. examined the effect of rigid and flexible catheters on the delivery of carboplatin and doxorubicin in both healthy and disease challenged rat brains, and found that the drug distributions delivered by the flexible catheters more closely approximated the theoretical ideal distribution from a point source than the distributions delivered by rigid catheters (Guarnieri et al. 2005). They hypothesize that this difference is caused by micro-tearing in the area around rigid catheters due to relative motion between the brain and the implant. Micro-tearing can create a high permeability path for fluid to escape the intended delivery area. Flexible catheters may be able move with the brain, thus eliminating micro-tearing and maintaining the close contact between the device and the tissue required for controlled delivery. This suggests that in treatments that use CED for chronic applications, flexible catheters could outperform traditional rigid devices. The feasibility of long term CED protocols has already been examined in clinical trials. A phase I trial examining the effect of year-long infusions of GDNF in Parkinson patients found that there were significant increases in dopamine storage in the putamen as a result of the treatment (Gill et al. 2003). However, subsequent phase II trials failed to replicate the success of that study (Lang et al. 2006). To determine why this trial failed, Salvatore and coworkers infused GDNF into the putamen of Rhesus monkeys for 7 days, and concluded that the trial had not been successful because the infusate localized around the tip of the catheter and did not distribute widely in the tissue (Salvatore et al. 2006). This result may be due to micro-tearing of the tissue around the implanted device. The use of a more flexible infusion catheter may reduce these problems and improve the efficacy of the treatment.

Treatment for the highly aggressive brain tumor glioblastoma multiforme also may benefit from the application of chronic CED protocols. This is an infiltrative tumor with cells that migrate away from the main tumor mass into healthy tissue (Holland 2000). In this case, CED is used to infuse chemotherapeutics into the tissue after the main tumor has been resected (Vogelbaum et al. 2007). It is also used as a xenograft model to test the effectiveness of new drugs under development (Saito et al. 2006; Krauze et al. 2007; Yamashita et al. 2007). In both of these cases, it would be useful to be able to deliver drugs repeatedly, based on tumor growth, at exactly the same location. It is very difficult to reinsert a needle or catheter for repeated applications of a drug at precisely the same location in tissue for a variety of reasons. Even if this were achieved, each insertion leaves a needle track that affects subsequent infusions. A chronically implantable device such as the one presented here is well-suited for repeated CED therapy.

Although flexible polymer microfluidic devices may demonstrate better long-term biocompatibility than silicon probes, their low rigidity makes them difficult to insert into tissue. To create chronic drug delivery implants that combine the desirable traits of small size and low rigidity, we constructed flexible parylene microfluidic devices supported by rigid scaffolds composed of poly(DL-lactide-*co*-glycolide) (PLGA, a biodegradable polyester). These scaffolds brace the flexible parylene device during insertion, but then degrade to leave the fluidic device in place in the tissue. Parylene was used for the microfluidic probe because it has many desirable characteristics. It has excellent dielectric properties (making it suitable for insulating electronics on the devices), it can be deposited using chemical vapor deposition (CVD) in uniform and consistent layers, and it is biologically compatible (meeting FDA class VI requirements). PLGA products are widely used in biomedical engineering applications as resorbable sutures (Chu 1982), orthopedic implants (Athanasiou et al. 1996), microspheres for controlled drug delivery (Cohen et al. 1991), and tissue engineering scaffolds (Mooney et al. 1996). PLGA structures are generally formed in two ways: through solvent removal techniques (Vozzi et al. 2003) and through thermal embossing, where the polymer is heated above its glass transition temperature and formed into the appropriate shape (King et al. 2004; Yang et al. 2005). In

this work the flexible microfluidic devices were constructed using top-down microfabrication techniques on a silicon wafer, and the degradable scaffolds were formed by hot-embossing the PLGA in a poly(dimethysiloxane) (PDMS) mold.

It has been found that PLGA structures display size-dependent degradation; larger structures undergo bulk degradation and smaller devices display only surface erosion (Grayson et al. 2005). As our scaffolds are close to the reported cut-off size that delineates bulk degradation and surface erosion, we examined the *in vitro* degradation time of the PLGA supports to determine how they degrade. We found that the scaffolds degrade with the manufacturer's reported degradation time, which suggests that they undergo bulk degradation.

The performance of the microfluidic devices was examined through infusions of dye into agarose gel brain phantoms and acute injections into the striatum of C57BL/6 mice. The devices were capable of penetrating tissue and delivering fluid in a controlled and reproducible way.

2 Materials and methods

2.1 Parylene microfluidic devices

The flexible parylene devices were produced on a silicon wafer using standard MEMS fabrication techniques. A schematic of the fabrication procedure is shown in Fig. 1(a). A CF_4 plasma was used to roughen the surface of a clean 100 mm single side polished silicon wafer before an 8 μm thick layer of parylene-C was deposited using chemical vapor deposition (PDS 2010 LabCoter, Specialty Coating Systems, Indianapolis IN). This layer formed the base of the fluidic device. Next, photoresist (Shipley 1045) was spun on the wafer to a depth of 11 μm (the intended height of the channels). This layer of photoresist was then patterned using contact lithography. The remaining photoresist defined the inside of the channels. A second 8 μm thick film of parylene-C was then deposited to form the top of the microfluidic device. Next, a 150 nm thick aluminum etch mask was deposited via e-beam evaporation (Mark 50 E-beam evaporation system, CHA Industries, Fremont CA). This mask was then patterned with a second photolithography step, and the exposed aluminum was removed via a wet-etch. An oxygen RIE (PlasmaLab 80+ RIE system, Oxford Instruments, Oxfordshire, UK) was then used to etch through the parylene to the silicon wafer, which defined the device body and opened the ends of the channels. Finally, the photoresist inside the channels was dissolved in acetone. The probes could then be easily peeled from the wafer to form free-standing parylene microfluidic devices.

2.2 Biodegradable insertion scaffolds

The PLGA insertion scaffolds were formed by hot-embossing PLGA granules in a poly(dimethylsiloxane) (PDMS) mold. To make the master mold, a silicon wafer was patterned using photolithography and selectively etched using a Bosch DRIE process (Unaxis SLR 770) to a depth of 200 μm. This wafer was then silanized with tridecaflouro – 1,2,2 tetrahydrooctyl trichlorosilane before the PDMS mold was cast to prevent the mold from bonding to the master. To cast the PDMS mold, PDMS base and curing agent (Sylgard 184 silicone elastomer kit, Dow

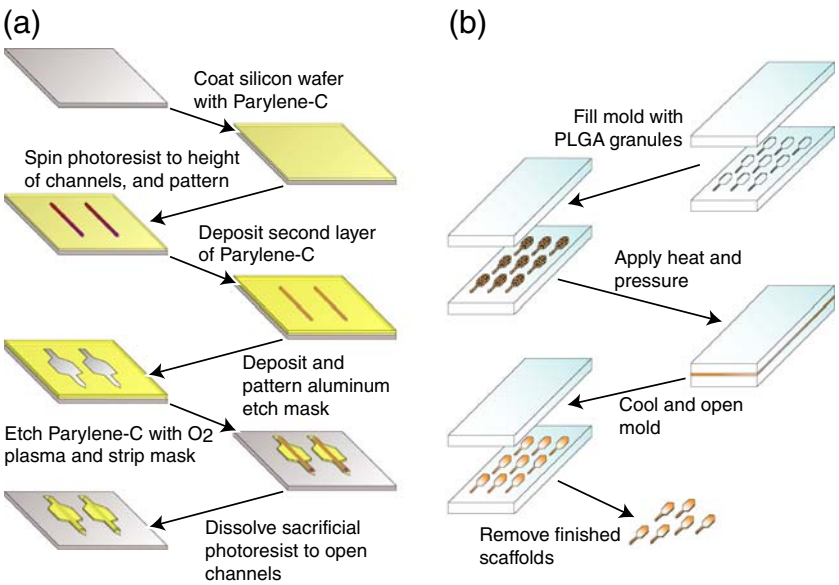

Fig. 1 Fabrication schematic for (**a**) flexible parylene microfluidic devices and, (**b**) PLGA insertion scaffolds

Corning, Midland MI) were mixed in a 10:1 weight ratio, and the mixture was thoroughly degassed. The mixture was then poured over the silicon master and cured at 70°C for 3 h. When the mold had cured, it could be peeled from the master and used for hot-embossing.

The scaffolds were formed using a method similar to that demonstrated by Yang et al (Yang et al. 2005). A schematic of the hot embossing procedure is shown in Fig. 1(b). Granules of PLGA (5050 DL 3.5A, Lakeshore Biomaterials, Birmingham AL) were placed on the mold and a second piece of non-patterned PDMS was placed on top. This sandwich was placed in a laboratory press with heated platens, heated to 150–160°C and pressed at approximately 3.5 MPa for 5–10 min. The assembly was cooled to below the glass transition temperature of the PLGA by circulating water through the platens. The sandwich was then disassembled, and the finished PLGA scaffolds could be cleanly removed from the mold.

2.3 Device assembly and *in vitro* characterization

To connect the microfluidic device to external tubing, one of the probe shanks was inserted into a 7 cm length of PEEK tubing (150 μm ID, 360 μm OD) (Upchurch Scientific, Oak Harbor WA) and sealed in place using a two-part epoxy (Epoxy 907, Miller-Stephenson, Danbury CT). The other end of the PEEK tubing was glued into the end of a borosilicate micropipette (1 mm OD, 0.58 mm ID) (World Precision Instruments Inc., Sarasota FL) using more epoxy. The parylene probe and PEEK tubing were fully primed under vacuum with the fluid to be infused; then the micropipette was backfilled using a syringe with a 28 gauge MicroFil needle tip (World Precision Instruments Inc.). The micropipette served as the fluidic reservoir for the parylene device. The proximal end of the glass micropipette was connected to a programmable pressure injector (PM8000, World Precision Instruments Inc.) using a micro-electrode holder. To infuse fluid using the parylene device, a constant pressure was applied to the fluidic reservoir in the micropipette via the pressure injector. The volumetric flow rate and infusion volume were determined by measuring the motion of the fluid meniscus in the lumen of the micropipette (speed and distance travelled, respectively).

To attach the microfluidic device to the insertion scaffold a small drop (~15 μl) of 5-min epoxy (Devcon, Danvers MA) was placed on the body of the scaffold and the primed microfluidic device was carefully laid on top under a stereoscope. The cured epoxy coupled the body of the scaffold to the body of the parylene device, leaving the shanks aligned but not connected. The shanks were then sealed together by briefly dipping them in dichloromethane. This treatment removes the highly permeable fluidic track between the two parts of the system. The device assembly was allowed to air dry for at least 15 min to ensure that all residual dichloromethane had evaporated, and thereby mitigate any negative biological effects that the dichloromethane treatment may cause. To allow the device to be inserted smoothly and reproducibly, the body of the scaffold/probe assembly was attached via double-sided adhesive tape to a custom made Delran block which was mounted on a micromanipulator.

This scaffold/microfluidic assembly was tested in a 0.6% wt/v agarose gel to verify that the scaffolds could penetrate tissue and that the microfluidic channels remained patent. The 0.6% wt/v agarose gel has similar mechanical properties as neural tissue, and is often used as a tissue phantom for *in vitro* device characterization (Chen et al. 2004). To examine the effect of dichloromethane treatment on the performance of the channels, the flow rates obtained for various driving pressures (6.9, 17.2, 34.5, 68.9, and 103.4 kPa) were compared before and after dichloromethane treatment.

2.4 PLGA scaffold degradation studies

In vitro degradation studies were carried out to determine the degradation time of the insertion scaffolds. PLGA scaffolds were weighed and placed in 50 mM HEPES buffer containing 10 mM KCl and 0.1% wt/v NaN3 (pH 7.4) and incubated at 37°C. Samples were removed every third day, washed, lyophilized and examined for gravimetric weight loss and molecular weight loss using GPC. The pH of the buffer was monitored and replaced with fresh buffer if the acidic degradation products caused the pH to drop below 7.3.

2.5 Acute *in vivo* infusions

Five male C57BL/6 mice weighing between 22 and 25 g were anesthetized by an intraperitoneal injection of ketamine/xylazine (0.1 mg/10 g mouse ketamine, 0.1 mg/10 g mouse xylazine). Animals were then secured in a stereotaxic frame, and an incision was made in the skin along the dorsal midline of the skull. A small craniotomy (3 mm diameter) was made over the left side of the exposed skull using a dental drill. The probe and attached scaffold were implanted using a micromanipulator 0.5 mm anterior, 2.5 mm lateral, and 3 mm deep from bregma. The device was then left for 2 min to allow the tissue to equilibrate before starting the infusion. Evan's Blue dye (2% wt/v in phosphate buffered saline) was infused using a starting infusion pressure of 0.69 kPa, and the infusion pressure was increased at a rate of 0.69 kPa/30 s to the final infusion pressure of 3.45 kPa. After 1 μl of dye had been injected, the infusion was stopped. The probe was left in the tissue for 2 min before being removed. The animal was removed from the stereotaxic frame and immediately sacrificed via cardiac injection of urethane. The brain was then promptly

extracted and frozen on dry ice. The frozen brain was sectioned into 20 μm thick slices on a cryostat and every third slice was retained for imaging. All procedures were carried out in accordance with the Cornell University Institutional Animal Care and Use Committee guidelines and regulations.

2.6 Image analysis

Tissue slices were imaged using a stereoscope and CCD camera. The captured RGB image files were analyzed using ImageJ software (NIH, Bethesda MD) and a custom macro. The macro adjusted the contrast of the image, and split the RGB image into its constituent colors. The macro then took the red channel of the image and converted the image to binary where the area stained with Evan's Blue dye was black, and the rest of the image was white. The threshold for this operation was determined by the ImageJ "getAutoThreshold" function which uses the Isodata algorithm (Abramoff et al. 2004). Next, noise was removed from image with a 3×3 pixel median filter. Finally, the area of the black pixels was summed to get the area of the Evan's Blue spot. The volume of distribution of the dye was calculated by summing the areas of distribution in each slice and multiplying the total by three times the slice thickness (to account for discarded sections).

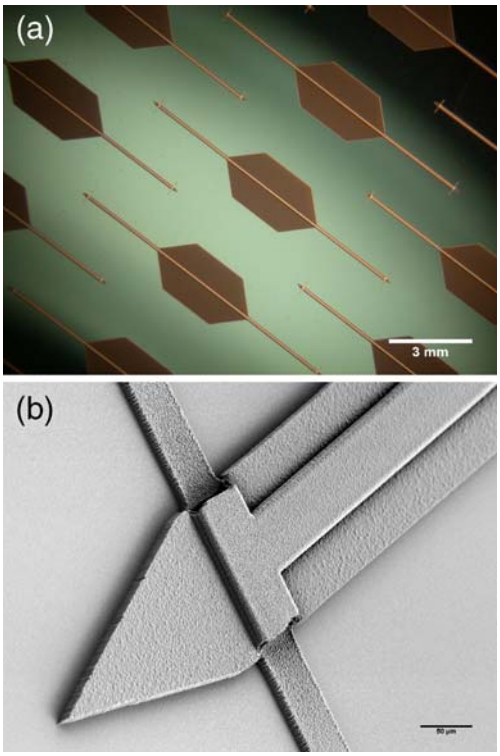

Fig. 2 (**a**) Whitelight image showing finished parylene microfluidic devices before they are removed from the silicon wafer. (**b**) Scanning electron micrograph of the tip of the flexible parylene device. Note the two channel openings. Scale bar is 50 μm

3 Results

3.1 Parylene probes and insertion scaffolds

The parylene microfluidic devices had an overall length of 10.3 mm and a 2 mm wide body for ease of handling. The insertable shank was 150 μm wide and 3.225 mm long (Fig. 2(a)). The devices were very flexible, and not rigid enough to penetrate tissue unaided. The microfluidic fluidic channel was 11.4 μm high, 50 μm wide, and had two openings at the inlet and outlet of the device to minimize occlusion (Fig. 2(b)).

The hot embossing technique was capable of rapidly producing highly uniform insertion scaffolds. The scaffolds were measured under an optical microscope and were slightly larger (< 10%) than the original silicon master, probably because of thermal expansion of the PDMS mold during the embossing process. Scanning electron micrographs of the scaffold shank and tip are shown in Fig. 3.

3.2 *In vitro* performance

The fluidic devices were easily inserted into agarose gel phantoms. Also, the dichloromethane treatment used to seal the shanks of the scaffold and parylene device together had no effect on the flow characteristics of the device. We infused dye solutions into the brain phantoms with negligible backflow, and the observed distributions closely approximated the spherical distribution of an ideal point source. Figure 4 shows the results of an infusion of green food dye into a 0.6% wt/v agarose gel brain phantom at a flow rate of approximately 0.1 μl/min.

3.3 PLGA scaffold degradation study

The scaffolds used in the degradation study had an average initial weight of 2.37±0.41 mg. The gravimetric weight loss as a function of time in the degradation buffer is shown in Fig. 5(a). Figure 5(b) shows the molecular weight loss as a function of time and represents the extent of hydrolysis in the polyester backbone of the scaffolds. The gravimetric weight loss is a representation of the rate that the oligomers formed by hydroloysis of the PLGA backbone escape from the bulk of the structure. The scaffolds were almost 100% degraded after 27 days, but were observed to be swollen and had no rigidity after only 15–18 days. This was comparable with the manufacturer's reported time (3–4 weeks), and indicates that these scaffolds are large enough to undergo bulk degradation rather than surface erosion.

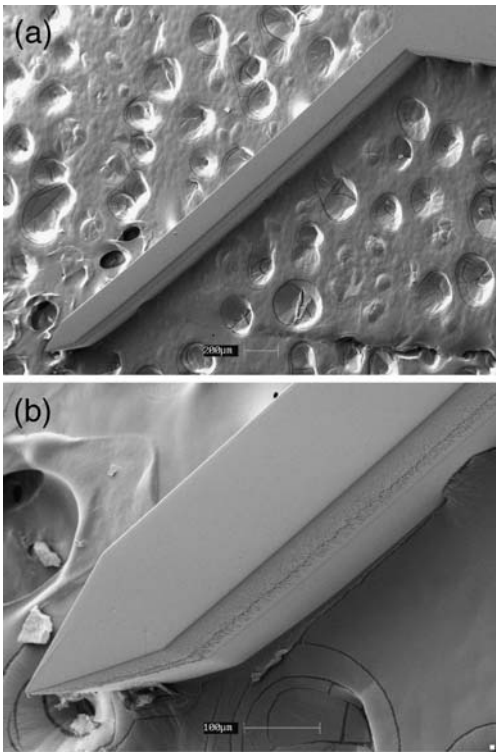

Fig. 3 Scanning electron micrographs showing the (**a**) insertable shank of the PLGA scaffold, and (**b**) the tip of the scaffold. Note the striations on the side of the device in (**b**). These are artifacts of the deep silicon etch used to define the master

3.4 *In vivo* performance

The parylene devices were used to infuse Evan's Blue dye into the striatum of mice. The system was able to easily penetrate the tissue, and was able to deliver fluid in a reproducible distribution. The average flow rate obtained in the *in vivo* experiments was 0.09±0.005 μl/min (n=5), at a driving pressure of 3.45 kPa.

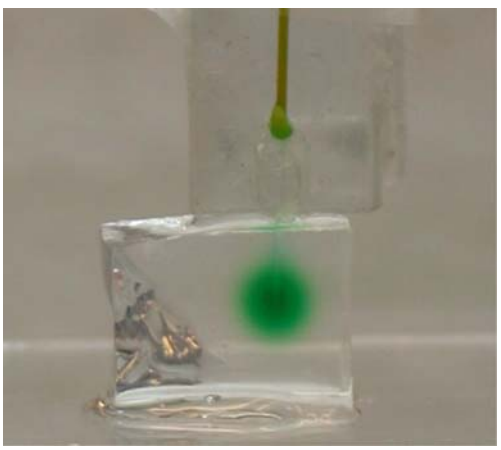

Fig. 4 Photograph showing results of a test infusion of green food dye into a 0.6% wt/v agarose gel brain phantom at a flow rate of 0.1 μl/min

The volume of distribution (V_d) of the infusate was 5.17 ± 0.36 mm^3 (n=5). Figure 6 shows an example of a brain section showing the distribution of Evan's Blue and the corresponding binary image that was used to determine the area of dye distribution in the section. Figure 7 shows a plot of the average area of the dye distribution in a section as a function of the square of the distance from the infusion site. For each replicate, the infusion site was defined as the tissue slice that showed the most extensive device insertion track, and the distance of any particular slice from the central axis of the infusion was calculated from the known thickness of the brain sections (20 μm). If the dye distribution volume can be represented as a body of revolution around an axis in the anterioposterior (AP) direction, the data presented in Fig. 7 should fall on a straight line (Neeves et al. 2007). If the distribution were a

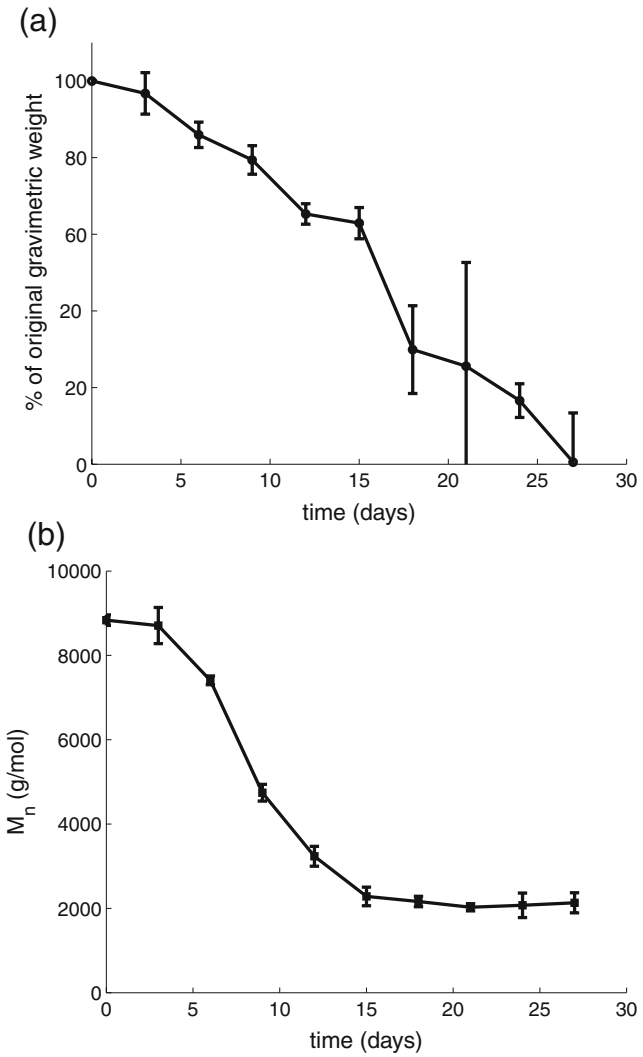

Fig. 5 (**a**) Gravimetric and (**b**) molecular weight loss of PLGA scaffolds as a function of time. Error bars represent the standard deviation of three replicates

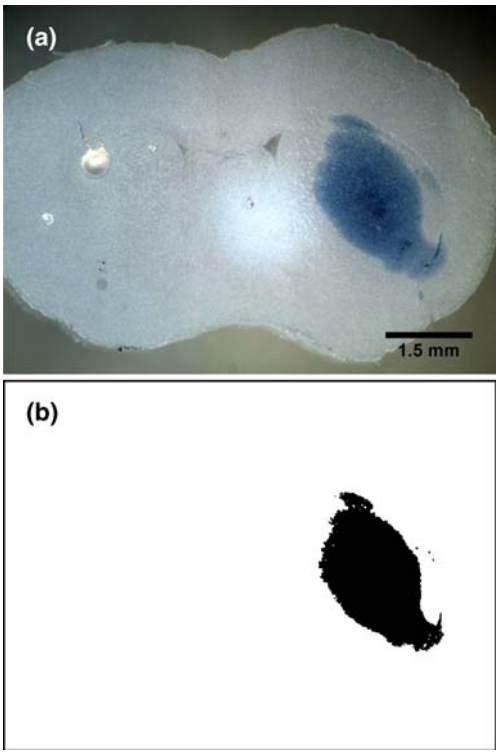

Fig. 6 Photograph of 20 μm thick coronal section of mouse brain tissue showing Evan's Blue distribution (**a**), and the corresponding binary image that was used to calculate the volume of distribution as part of a series of sections (**b**)

perfect sphere, the line would have slope π. Areas of the plot in Fig. 7 with a slope equal to ±π correspond to regions where the distribution is isotropic. Deviations from this slope indicate regions of anisotropic distribution.

4 Discussion

The parylene microfluidic devices in this study were capable of infusing fluids in mouse striatum at flow rates that are relevant for convection enhanced delivery. The maximum flow rate that can be achieved in CED often is determined by the onset of backflow along the outside of the needle or catheter. Morrison et al (Morrison et al. 1999) showed that the length of backflow is directly proportional to the volumetric flow rate imposed and the radius of the infusion catheter. Owing to the small size of the C57BL/6 mouse striatum, the maximum flow rate achieved in these experiments was 0.09 μl/min. At higher flow rates, backflow along the outside of the device reached the corpus collosum, which is only 1.6 mm from the tip of the device in the mouse (Rosen et al. 2000). Although 0.09 μl/min is lower than flow rates used in CED studies in humans (e.g. 2–12 μl/min, (Mardor et al. 2001; Lidar et al. 2004; Kunwar et al. 2007; Sampson et al. 2003; Weber et al. 2003; Worgall et al. 2008; Ren et al. 2003), it is comparable to flow rates used by groups that have studied CED in mice using conventional needles (Oh et al. 2007). Furthermore, it is reasonable to expect that higher infusion rates could be achieved without backflow using a parlyene device with a longer shank in larger animals. In any event, the data show that the parylene/PLGA system is capable of delivering fluid in a controlled and reproducible way. The ratio of the volume distributed (V_d) to the volume infused (V_i) was 5.17 (n=5), with a standard deviation of 0.36 (6.9% of the mean). This value is close to the theoretical value obtained for the free volume of the tissue given a porosity of 0.2 (Nicholson 2001), which suggests that the parylene/PLGA system distributed all of the infused fluid to the available extracellular space of the tissue. Furthermore, the results presented in Fig. 7 show that the distribution volume closely approximates the ideal spherical distribution associated with infusion from a point source.

The slight increase in size of the scaffolds when compared with that of the original silicon master is likely due to thermal expansion and pressure induced deformation of the PDMS mold during hot embossing. This effect was also observed by Yang et al (Yang et al. 2005).

The degradation time of the scaffolds in this study was determined *in vitro* to be 27 days, which was consistent with the manufacturers reported value (3–4 weeks). Grayson et al found that the sample size affected its degradation time; larger samples were subject to bulk degradation, which accelerated their degradation compared with smaller samples that degraded primarily by surface erosion (Grayson et al. 2005). In our case the scaffolds were large enough to undergo bulk degradation and therefore exhibited the manufacturer's reported degradation time.

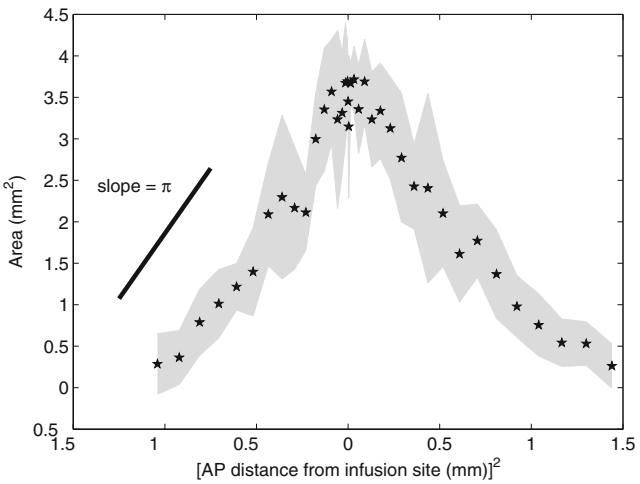

Fig. 7 The average area of dye distribution in each brain section as a function of the square of the distance from the infusion site. The shaded region represents the standard deviation of the data (n=5). A line with slope π is shown for reference. Areas of the plot with a slope equal to ±π correspond to a region where the distribution is isotropic. Deviations from this slope indicate anisotropic distributions

Long term *in vitro* phantom studies were not carried out on the device, because the space around the degraded scaffold provides a high permeability zone for fluid to escape the gel, precluding the possibility of obtaining information about the long term *in vitro* fluid delivery performance of the microfluidic devices. This is not expected to be a problem in chronic *in vivo* experiments as the local tissue would infiltrate the volume occupied by the scaffold as it erodes, filling the void space left by the scaffold.

PLGA structures have a long history of use in controlled release drug delivery devices (Sanders et al. 1986) and their release characteristics have been well characterized. The insertion scaffolds could easily be loaded with drugs that might influence the local tissue to improve the effectiveness of the CED protocol, e.g. the controlled release of dexamethasone to mediate inflammation (Shain et al. 2003; Spataro et al. 2005). To date, we have successfully loaded the PLGA scaffolds with up to 15% wt/wt dexamethasone to examine the effect of local diffusive release of drug on the chronic performance of the parylene devices. Also, the degradation time of the scaffolds could be readily adjusted by changing the molecular weight of the PLGA, by changing the end group, or by changing the lactide to glycolide ratio. This, in turn, could be used to control the duration of any local controlled release, which makes this a promisingly tunable system.

This study also shows that a flexible microdevice can be inserted into tissue using an external PLGA scaffold to stiffen the probe. The external scaffold increases the effective 2nd moment of area of the system, providing enough buckling resistance to penetrate the tissue, before degrading to leave the smaller parylene device free to deform with bulk motion of the brain. A simple analysis of the critical load for Euler buckling of the device provides insight into design requirements of a larger system to deliver fluid in bigger animals. By modeling the device as a parylene strip 20 μm high by 150 μm wide, attached to a PLGA beam that is 150 μm wide and 200 μm tall the parallel axis theorem can be used to determine the effective second moment of area of the parylene/PLGA device to be 1.39×10^{-16} m^4. The effective Young's modulus of the device was found to be 1.67 GPa. This was determined by multiplying the individual Young's moduli of the PLGA (1.31 GPa, from Lakeshore Biomaterials company website) and parylene (2.76 GPa, Specialty Coating Systems company website) by the second moment of area of the respective PLGA and parylene device sections, and dividing the total by the effective second moment of area of the overall device. The result was used to determine the theoretical critical Euler buckling load of the system to be 55 mN, based on an unsupported device length of 3.225 mm and a fixed-free end arrangement. In order to use this system to deliver fluid to the caudate of a rat, the device length must be increased by a factor of two owing to the size of the rat brain. To maintain the same critical buckling load while doubling the unsupported length of the shanks would require the PLGA scaffold to be 150 μm wide and 340 μm high.

The method presented here may be of use to researchers developing flexible neural electrodes for chronic applications. Takeuchi et al (Takeuchi et al. 2005) used poly (ethylene glycol) (PEG) as a stiffening agent for flexible neural probes. In their technique a fluidic channel on the device is backfilled with molten PEG, which solidifies and stiffens the device enough to allow it to be inserted into tissue. The PEG then dissolves once the device is implanted. However, their devices were tested in the cortex of rats, so it is unclear whether the PEG is rigid enough to allow the devices to be inserted accurately into deep tissue structures. Furthermore, their method requires the implantable device to have a relatively large fluidic channel that can be backfilled with molten PEG. The use of an external PLGA scaffold would not require a fluidic channel if recording/stimulating electrodes were all that were needed, which would simplify the fabrication. Moreover, the dichloromethane application step is not required if infusions are not being performed, further simplifying the use of this system.

5 Conclusions

This study is a first step toward a device that can be used in studies of chronic CED therapy. The results show that it is possible to implant flexible polymeric devices deep into neurological tissue, and to use these implanted devices to deliver fluid in a controlled and reproducible manner. The methods developed here could be easily adapted for implantation of other types of flexible neural microprobes.

Future work on this system will compare the long-term performance and biocompatibility of the parylene/PLGA system in chronic implants (with and without local diffusive delivery of therapeutics from the scaffolds) with those of silicon microprobes and conventional catheters. The devices will also be lengthened to permit their use in larger rodent models.

Acknowledgements The authors thank Eric Chang for his assistance with this work, and Dr. Jonathan T. Butcher for helpful discussions. This work was supported by the National Institutes of Health Grant NS-045236. This work was performed in part at the Cornell Nano-Scale Facility, a member of the National Nanotechnology Infrastructure Network, which is supported by the National Science Foundation (Grant ECS-0335765). Also, this work made use of STC shared experimental facilities supported by the National Science Foundation under Agreement No. ECS-9876771.

References

M. Abramoff, P. Magalhaes, S. Ram, Biophotonics Int. **11**, 36 (2004)

K.A. Athanasiou, G.G. Niederauer, C.M. Agrawal, Biomaterials. **17**, 93 (1996). doi:10.1016/0142-9612(96)85754-1

R.H. Bobo, D.W. Laske, A. Akbasak, P.F. Morrison, R.L. Dedrick, E.H. Oldfield, Proc. Natl. Acad. Sci. USA. **91**, 2076 (1994). doi:10.1073/pnas.91.6.2076

J. Chen, K.D. Wise, J.F. Hetke, S.C. Bledsoe, IEEE Trans. Biomed. Eng. **44**, 760 (1997). doi:10.1109/10.605435

Z.-J. Chen, G.T. Gillies, W.C. Broaddus, S.S. Prabhu, H. Fillmore, R.M. Mitchell, F.D. Corwin, P.P. Fatouros, J. Neurosurg. **101**, 314 (2004)

C.C. Chu, J. Biomed. Mater. Res. **16**, 117 (1982). doi:10.1002/jbm.820160204

S. Cohen, T. Yoshioka, M. Lucarelli, L.H. Hwang, R. Langer. Pharm. Res. **8**, 713 (1991). doi:10.1023/A:1015841715384

S.S. Gill, N.K. Patel, G.R. Hotton, K. O'Sullivan, R. McCarter, M. Bunnage, D.J. Brooks, C.N. Svendsen, P. Heywood. Nat. Med. **9**, 589 (2003). doi:10.1038/nm850

A.C.R. Grayson, M.J. Cima, R. Langer, Biomaterials. **26**, 2137 (2005). doi:10.1016/j.biomaterials.2004.06.033

D.R. Groothuis, S. Ward, A.C. Itskovich, C. Dobrescu, C.V. Allen, C. Dills, R.M. Levy, J. Neurosurg. **90**, 321 (1999)

D.R. Groothuis, H. Benalcazar, C.V. Allen, R.M. Wise, C. Dills, C. Dobrescu, V. Rothholtz, R.M. Levy, Brain Res. **856**, 281 (2000). doi:10.1016/S0006-8993(99)02089-2

M. Guarnieri, B.S. Carson, A. Khan, M. Penno, G.I. Jallo, J. Neurosci. Methods. **144**, 147 (2005)

M.F. Haller, W.M. Saltzman, Pharm. Res. **15**, 377 (1998). doi:10.1023/A:1011911912174

J.F. Hamilton, P.F. Morrison, M.Y. Chen, J. Harvey-White, R.S. Pernaute, H. Phillips, E. Oldfield, K.S. Bankiewicz, Exp. Neurol. **168**, 155 (2001). doi:10.1006/exnr.2000.7571

E.C. Holland, Proc. Natl. Acad. Sci. USA. **97**, 6242 (2000). doi:10.1073/pnas.97.12.6242

Y. Kim, R. Hitchcock, M. Bridge, P. Tresco. Biomaterials. **25**, 2229 (2004). doi:10.1016/j.biomaterials.2003.09.010

K. King, C. Wang, M. Kaazempur-Mofrad, J. Vacanti, J. Borenstein. Adv. Mater. **16**, 2007 (2004). doi:10.1002/adma.200306522

M.T. Krauze, C.O. Noble, T. Kawaguchi, D. Drummond, D.B. Kirpotin, Y. Yamashita, E. Kullberg, J. Forsayeth, J.W. Park, K.S. Bankiewicz, Neuro-oncol. **9**, 393 (2007). doi:10.1215/15228517-2007-019

C.E. Krewson, W.M. Saltzman, Brain Res. **727**, 169 (1996). doi:10.1016/0006-8993(96)00378-2

S. Kunwar, M.D. Prados, S.M. Chang, M.S. Berger, F.F. Lang, J.M. Piepmeier, J.H. Sampson, Z. Ram, P.H. Gutin, R.D. Gibbons, K.D. Aldape, D.J. Croteau, J.W. Sherman, R.K. Puri, C.B.I.S. Group, J. Clin. Oncol. **25**, 837 (2007). doi:10.1200/JCO.2006.08.1117

A.E. Lang, S. Gill, N.K. Patel, A. Lozano, J.G. Nutt, R. Penn, D.J. Brooks, G. Hotton, E. Moro, P. Heywood, M.A. Brodsky, K. Burchiel, P. Kelly, A. Dalvi, B. Scott, M. Stacy, D. Turner, V.G.F. Wooten, W.J. Elias, E.R. Laws, V. Dhawan, A.J. Stoessl, J. Matcham, R.J. Coffey, M. Traub. Ann. Neurol. **59**, 459 (2006). doi:10.1002/ana.20737

D.W. Laske, P.F. Morrison, D.M. Lieberman, M.E. Corthesy, J.C. Reynolds, P.A. Stewart-Henney, S.S. Koong, A. Cummins, C.H. Paik, E.H. Oldfield, J. Neurosurg. **87**, 586 (1997)

Z. Lidar, Y. Mardor, T. Jonas, R. Pfeffer, M. Faibel, D. Nass, M. Hadani, Z. Ram, J. Neurosurg. **100**, 472 (2004)

D.M. Lieberman, D.W. Laske, P.F. Morrison, K.S. Bankiewicz, E.H. Oldfield, J. Neurosurg. **82**, 1021 (1995)

R.R. Lonser, M.E. Corthésy, P.F. Morrison, N. Gogate, E.H. Oldfield, J. Neurosurg. **91**, 294 (1999)

R.R. Lonser, S. Walbridge, K. Garmestani, J.A. Butman, H.A. Walters, A.O. Vortmeyer, P.F. Morrison, M.W. Brechbiel, E.H. Oldfield, J. Neurosurg. **97**, 905 (2002)

Y. Mardor, Y. Roth, Z. Lidar, T. Jonas, R. Pfeffer, S.E. Maier, M. Faibel, D. Nass, M. Hadani, A. Orenstein, J.S. Cohen, Z. Ram. Cancer Res. **61**, 4971 (2001)

D.J. Mooney, C.L. Mazzoni, C. Breuer, K. McNamara, D. Hern, J.P. Vacanti, R. Langer. Biomaterials. **17**, 115 (1996). doi:10.1016/0142-9612(96)85756-5

P.F. Morrison, M.Y. Chen, R.S. Chadwick, R.R. Lonser, E.H. Oldfield, J. Am. Physiol. **277**, R1218 (1999)

K.B. Neeves, C.T. Lo, C.P. Foley, W.M. Saltzman, W.L. Olbricht, J. Control. Release. **111**, 252 (2006). doi:10.1016/j.jconrel.2005.11.018

K.B. Neeves, A.J. Sawyer, C.P. Foley, W.M. Saltzman, W.L. Olbricht, Brain Res. **1180**, 121 (2007). doi:10.1016/j.brainres.2007.08.050

C. Nicholson, Rep. Prog. Phys. **64**, 815 (2001). doi:10.1088/0034-4885/64/7/202

S. Oh, R. Odland, S.R. Wilson, K.M. Kroeger, C. Liu, P.R. Lowenstein, M.G. Castro, W.A. Hall, J.R. Ohlfest, J. Neurosurg. **107**, 568 (2007)

R. Rathnasingham, D.R. Kipke, S.C. Bledsoe, J.D. McLaren, IEEE Trans. Biomed. Eng. **51**, 138 (2004). doi:10.1109/TBME.2003.820311

H. Ren, T. Boulikas, K. Lundstrom, A. Söling, P.C. Warnke, N.G. Rainov, J. Neurooncol. **64**, 147 (2003)

G. Rosen, A. Williams, J. Capra, M. Connolly, B. Cruz, L. Lu, D. Airey, K. Kulkarni, R. Williams, The mouse brain library@www.mbl.org. in *Int Mouse Genome Conference* (2000) vol. 14, p. 166

P. Rousche, D. Pellinen, D. Pivin Jr., J. Williams, R. Vetter, IEEE Trans. Biomed. Eng. **48**, 361 (2001)

R. Saito, M.T. Krauze, C.O. Noble, D.C. Drummond, D.B. Kirpotin, M.S. Berger, J.W. Park, K.S. Bankiewicz, Neuro. Oncol. **8**, 205 (2006)

M.F. Salvatore, Y. Ai, B. Fischer, A.M. Zhang, R.C. Grondin, Z. Zhang, G.A. Gerhardt, D.M. Gash, Exp. Neurol. **202**, 497 (2006)

J.H. Sampson, G. Akabani, G.E. Archer, D.D. Bigner, M.S. Berger, A. H. Friedman, H.S. Friedman, J.E. Herndon, S. Kunwar, S. Marcus, R.E. McLendon, A. Paolino, K. Penne, J. Provenzale, J. Quinn, D.A. Reardon, J. Rich, T. Stenzel, S. Tourt-Uhlig, C. Wikstrand, T. Wong, R. Williams, F. Yuan, M.R. Zalutsky, I. Pastan, J. Neurooncol. **65**, 27 (2003)

L.M. Sanders, B.A. Kell, G.I. McRae, G.W. Whitehead, J. Pharm. Sci. **75**, 356 (1986)

W. Shain, L. Spataro, J. Dilgen, K. Haverstick, S. Retterer, M. Isaacson, M. Saltzman, J.N. Turner, IEEE Trans. Neural. Syst. Rehabil. Eng. **11**, 186 (2003)

L. Spataro, J. Dilgen, S. Retterer, A.J. Spence, M. Isaacson, J.N. Turner, W. Shain, Exp. Neurol. **194**, 289 (2005)

J. Subbaroyan, D.C. Martin, D.R. Kipke, J. Neural. Eng. **2**, 103 (2005)

D.H. Szarowski, M.D. Andersen, S. Retterer, A.J. Spence, M. Isaacson, H.G. Craighead, J.N. Turner, W. Shain, Brain Res. **983**, 23 (2003)

S. Takeuchi, D. Ziegler, Y. Yoshida, K. Mabuchi, T. Suzuki, Lab. Chip. **5**, 519 (2005)

J.N. Turner, W. Shain, D.H. Szarowski, M. Andersen, S. Martins, M. Isaacson, H. Craighead, Exp. Neurol. **156**, 33 (1999)

M.A. Vogelbaum, J.H. Sampson, S. Kunwar, S.M. Chang, M. Shaffrey, A.L. Asher, F.F. Lang, D. Croteau, K. Parker, A.Y. Grahn, J.W. Sherman, S.R. Husain, R.K. Puri, Neurosurgery. **61**, 1031 (2007)

G. Vozzi, C. Flaim, A. Ahluwalia, S. Bhatia, Biomaterials. **24**, 2533 (2003)

K.A. Walter, M.A. Cahan, A. Gur, B. Tyler, J. Hilton, O.M. Colvin, P.C. Burger, A. Domb, H. Brem, Cancer Res. **54**, 2207 (1994)

F. Weber, A. Asher, R. Bucholz, M. Berger, M. Prados, S. Chang, J. Bruce, W. Hall, N.G. Rainov, M. Westphal, R.E. Warnick, R.W. Rand, F. Floeth, F. Rommel, H. Pan, V.N. Hingorani, R.K. Puri, J. Neurooncol. **64**, 125 (2003)

S. Worgall, D. Sondhi, N.R. Hackett, B. Kosofsky, M.V. Kekatpure, N. Neyzi, J.P. Dyke, D. Ballon, L. Heier, B.M. Greenwald, P. Christos, M. Mazumdar, M.M. Souweidane, M.G. Kaplitt, R.G. Crystal, Hum. Gene. Ther. **19**, 463 (2008)

Y. Yamashita, M.T. Krauze, T. Kawaguchi, C.O. Noble, D.C. Drummond, J.W. Park, K.S. Bankiewicz, Neuro. Oncol. **9**, 20 (2007)

W. Yang, R.F. Barth, D.M. Adams, M.J. Ciesielski, R.A. Fenstermaker, S. Shukla, W. Tjarks, M.A. Caligiuri, Cancer Res. **62**, 6552 (2002)

Y. Yang, S. Basu, D.L. Tomasko, L.J. Lee, S.-T. Yang, Biomaterials. **26**, 2585 (2005)